Strong correspondence principle and the classical-resonance overlap criterion for the onset of chaos

Bala Sundaram* and R. V. Jensen†
Department of Physics and Center for Theoretical Physics, Texas A&M University, College Station, Texas 77843-4242
(Received 18 July 1994)

The overlap of classical resonances has been particularly successful in predicting ionization thresholds for hydrogen atoms in strong microwave fields, although not for low scaled frequencies. In this paper, we explicitly relate quantum mechanically computed matrix elements to the classical Fourier amplitudes used in the overlap criterion. The resulting twist to this demonstration of classical-quantum correspondence is that quantum matrix elements can be used to improve predictions of classical-resonance overlap for low scaled frequencies. Conversely, the classical amplitudes are shown to contain delicate cancellations in the quantum matrix elements. In the course of this demonstration, we also introduce a compact numerical method for evaluating high-order multiphoton matrix elements.

PACS number(s): 32.80.Rm, 05.45.+b, 42.50.Hz

I. INTRODUCTION

The classical-resonance overlap criterion provides a very powerful tool for determining the conditions for the onset of chaos in periodically driven nonlinear oscillators [1]. In particular, the early application to periodically perturbed Kepler orbits provided estimates for the critical microwave fields for the chaotic ionization of highly excited hydrogen atoms [2–4], which were in remarkable agreement with the experimental measurements on real hydrogen atoms [5,6]. Combined with detailed numerical studies of the classical and quantum dynamics of this strongly perturbed atomic system [6–10], this pioneering work has stimulated much research activity in the new frontier of "quantum chaos" over the past decade.

The resonance overlap criterion for periodically perturbed nonlinear oscillators is based on classical perturbation theory. It uses the Fourier coefficients of the perturbation to estimate the widths of resonances in the classical action-angle space of the nonlinear oscillator [1,2]. Widespread or global chaos arises in the dynamics of the perturbed oscillator when these resonances overlap. The key to using this criterion is the accurate location of the classical-resonances and the calculation of their widths. The purpose of this paper is to illustrate a procedure for determining the classical-resonance widths using the Heisenberg strong correspondence principle [11] to relate the classical Fourier coefficents to quantum mechanical matrix elements. This procedure may be particularly effective when the classical canonical transformation for obtaining the resonance widths is very complicated as in the case of the perturbation of highly excited hydrogen atoms (with principle quantum number n) using microwave frequencies, Ω, less than the natural oscillation frequency $1/n^3$. Specifically, we show that the quantum mechanical matrix elements for multiphoton transitions in the strongly perturbed hydrogen atom can be used to extend the resonance overlap criterion to accurately estimate the threshold microwave fields for the onset of chaotic ionization at low scaled frequencies, $n^3\Omega < 1$.

Of course, the relatively crude resonance overlap criterion is not a panacea. It is intended only to give a rough (factor of 2) estimate of the conditions for the classical transition from stable, bound-electron motion to unstable dynamics that can lead to ionization. In addition, detailed studies of the classical-quantum correspondence in the microwave ionization experiments reveal a number of subtle discrepancies [12,13] that continue to challenge the theoretical interpretation of the experimental measurements. Nevertheless, as a first approximation the resonance overlap criterion provides an excellent estimate of the magnitude and parameter dependence of the transition to global chaos that can serve to guide both experimental and theoretical studies of the transition to chaos in classical nonlinear oscillators and investigations of the behavior of the corresponding quantum systems.

Section II begins with a formal development of the classical-resonance overlap criterion for the onset of chaotic ionization at low scaled frequencies, which is a generalization of an approach first introduced by Blümel and Smilansky [9]. In Sec. III we comment on the remarkable correspondence between the classical Fourier coefficients of the perturbation and the quantum multiphoton matrix elements for this system, which is a consequence of the Heisenberg strong correspondence principle [11]. In particular, the classical Fourier amplitudes automatically yield accurate estimates for the quantum multiphoton matrix elements that were previously shown [14,15] to require delicate cancellations involving competing terms orders of magnitude larger than the final

*Present address: Department of Physics, University of Texas at Austin, Austin, TX 78712.
†Present address: Department of Physics, Wesleyan University, Middletown, CT 06459.

result. This classical-quantum correspondence suggests in turn that the quantum multiphoton matrix elements may provide an accurate and effective means of estimating the classical Fourier coefficients that determine the island widths for low-frequency resonances. In Sec. IV an efficient algorithm for calculating the multiphoton matrix elements is described. These quantum mechanical matrix elements are then used to improve the estimates of the classical Fourier amplitudes utilized in the resonance overlap criterion developed in Sec. II for the low-frequency microwave ionization of highly excited hydrogen atoms. Finally, rules for extracting the dominant contributions to the classical resonance widths as well as schemes for evaluating the multiphoton matrix elements within MATHEMATICA [16] are contained in the Appendixes.

II. RESONANCE OVERLAP THEORY FOR $n^3\Omega < 1$

We start with the Hamiltonian for the one-dimensional (1D) hydrogen atom in an oscillating electric field:

$$H(x,p,t) = p^2/2 + \left\{ \begin{array}{ll} -1/x, & x > 0 \\ \infty, & x \leq 0 \end{array} \right\} + xF\cos(\Omega t) \ . \tag{1}$$

On transforming to the action angle variables for the unperturbed Hamiltonian:

$$H(\theta,I,t) = -1/2I^2 + F\sum_{m=-\infty}^{\infty} V_m(I)\cos\left(m\theta - \Omega t\right) \ , \tag{2}$$

where $V_m(I) \equiv C_{\rm Cl}(m)I^2$ with coefficients

$$C_{\rm Cl}(m) = \left\{ \begin{array}{ll} \frac{3}{2}, & m = 0 \\ -J'_m(m)/m, & m \neq 0. \end{array} \right. \tag{3}$$

Hamilton's equations of motion for the action and angle variables are

$$\frac{dI}{dt} = F\sum_{m\neq 0} mV_m(I)\sin\left(m\theta - \Omega t\right), \tag{4}$$

$$\frac{d\theta}{dt} = 1/I^3 + F\sum_{m=-\infty}^{\infty} V'_m(I)\cos\left(m\theta - \Omega t\right) \ . \tag{5}$$

Formally integrating to lowest order in a perturbation expansion in F, the solutions are

$$I(t) = I_0 + F\sum_{m\neq 0}\frac{mV_m(I_0)}{(m\Omega_0 - \Omega)}\cos[(m\Omega_0 - \Omega)t] + O(F^2), \tag{6}$$

$$\theta(t) = \theta_0 + \Omega_0 t + F\sum_{m=-\infty}^{\infty}\frac{V'_m(I_0)}{(m\Omega_0 - \Omega)}\sin[(m\Omega_0 - \Omega)t] + O(F^2), \tag{7}$$

where I_0 and θ_0 are the initial values of the action-angle variables and

$$\Omega_0 = 1/I^3|_{I=I_0} \tag{8}$$

is the classical Kepler orbital frequency.

This result suggests that we isolate the leading oscillatory perturbations by introducing a new angle variable

$$\phi = \theta - F\sum_{k=-\infty}^{\infty} b_k \sin[(k\Omega_0 - \Omega)t] \ , \tag{9}$$

where

$$b_k = V'_k(I)/(k\Omega_0 - \Omega) = \left\{ \begin{array}{ll} -3I/\Omega, & k = 0 \\ -2IJ'_k(k)/k(k\Omega_0 - \Omega), & k \neq 0. \end{array} \right. \tag{10}$$

At first we keep the action variable unchanged using the generating function

$$F_2(\theta,I,t) = I\theta - F\sum_{m=-\infty}^{\infty}\int_0^I b_m(I)\sin[(m\Omega_0 - \Omega)t]dI \ . \tag{11}$$

Then the new Hamiltonian is

$$K(\phi,I,t) = -1/2I^2 + F\sum_{m=-\infty}^{\infty} V_m(I)\cos\left[m\left(\phi + F\sum_{k=-\infty}^{\infty} b_k\sin[(k\Omega_0 - \Omega)t]\right) - \Omega t\right] + \partial F_2/\partial t \ . \tag{12}$$

(Note that since $\partial F_2/\partial t$ does not depend on θ or ϕ this term will not contribute to any new classical resonances. Furthermore, the $m = 0$ term in $\partial F_2/\partial t$ term exactly cancels the remaining $m = 0$ term in the new Hamiltonian.)

For large driving frequencies, $\Omega/\Omega_0 > 1$, a good description of the critical fields for the onset of global chaos can be achieved by neglecting the higher-order resonances by setting all $b_k = 0$ in Eq. (12) [17,18]. In this case dynamical resonances occur only for $\Omega/\Omega_0 \approx m$ with $m = 0, \pm 1, \pm 2, \ldots$, where the phases of the remaining oscillatory terms in Eq. (12) are stationary.

However, for low driving frequencies, $\Omega/\Omega_0 < 1$, the additional resonant interactions at subharmonic frequencies with $\Omega/\Omega_0 = 1/q$ must also be included. In particular, if we expand the cosine of the sine in Eq. (12) in terms of Bessel functions, then the full Hamiltonian can be expressed in a form that clearly exposes the higher-order, subharmonic resonances that determine the resonance overlap criterion for the onset of global chaos for $n^3\Omega < 1$:

$$K(\phi, I, t) = -1/2I^2 + F \sum_{m=-\infty}^{\infty} V_m(I)\ \mathrm{Re}\left(e^{i(m\phi - \Omega t)} \prod_{k=-\infty}^{\infty} \sum_{s_k=-\infty}^{\infty} J_{s_k}(mFb_k) e^{is_k(k\Omega_0 - \Omega)t} \right) + \partial F_2/\partial t\ . \tag{13}$$

This Hamiltonian is still exact. Although the infinite product of the infinite sums of Bessel functions appears complicated, a typical term of the perturbed part of the Hamiltonian K corresponding to a "string" of indices m, k, and $\{s_k\}_{k=-\infty,\infty}$ can be simply expressed in terms of an amplitude and a phase

$$A_m(k, \{s_k\}) \cos\left[m\phi - \left(\Omega - \sum_{s_k=-\infty}^{\infty} s_k(k\Omega_0 - \Omega) \right) t \right] , \tag{14}$$

where the Fourier amplitude is expressed in terms of products of Bessel functions,

$$A_m(k, \{s_k\}) = FV_m(I) \prod_{\{s_k\}} J_{s_k}(mFb_k)\ . \tag{15}$$

By approximating $\phi \approx \Omega_0 t$, the resonances associated with each of these terms can be determined by the condition that the phases in Eq. (14) be stationary

$$m\Omega_0 - \left(\Omega - \sum_{s_k=-\infty}^{\infty} s_k(k\Omega_0 - \Omega) \right) = 0. \tag{16}$$

This occurs when the ratio of the perturbation frequency, Ω, to the natural frequency, $\Omega_0 = 1/I^3$, is

$$\Omega/\Omega_0 = I^3\Omega = \left(m + \sum_{s_k=-\infty}^{\infty} k s_k \right) \Big/ \left(1 + \sum_{s_k=-\infty}^{\infty} s_k \right) . \tag{17}$$

Since m, k, $\{s_k\}$ are all integers, the resonances occur when $I^3\Omega$ is a rational ratio p/q.

Consider for example the case $I^3\Omega = 1/q < 1$. Then the resonant action is

$$I_{1/q} = (1/q\Omega)^{\frac{1}{3}}. \tag{18}$$

The resonance width about this action is determined by the Fourier amplitudes $A_m(k, \{s_k\})$ defined by Eq. (15) corresponding to strings of m, k, $\{s_k\}$ that satisfy Eq. (17), that is,

$$m + \sum_{s_k=-\infty}^{\infty} k s_k = 1, \tag{19}$$

$$1 + \sum_{s_k=-\infty}^{\infty} s_k = q\ . \tag{20}$$

As the magnitude of the Bessel functions decreases rapidly with increasing order for small arguments, only a few of the many factors in Eq. (15) contribute to the amplitude of these resonances. In fact, a careful analysis of the relative size of these factors shows that the dominant terms for $q = 1, \ldots, 10$ come from index strings with (a) $m = 1$ (since $V_m \sim 1/m^{\frac{5}{3}}$), (b) the largest value of s_0 that satisfies the resonance condition, Eq. (20) (since $b_0 \gg b_{k\neq 0}$), and (c) $1 + \sum_{s_k=-\infty}^{\infty} |s_k| = q$ (since the small argument expansion of the Bessel functions then gives $A_{m,\{s_k\}} \sim F^q$). (Note that this last condition neglects counterrotating terms with $m < 0$.)

Application of the rules (a), (b), and (c) shows that the leading term for $\Omega/\Omega_0 = 1/q$ with $q = 1, \ldots, 10$ corresponds to the index string

$$m = 1, \quad s_0 = q - 1, \quad s_{k\neq 0} = 0\ . \tag{21}$$

Since $J_0 \sim 1$ for small arguments, the leading contribution to the amplitude of the $1/q$ resonance comes from

$$A_1^{(q)} = FV_1(I) J_{q-1}(-3qF_0)\ , \tag{22}$$

where $F_0 \equiv I^4F$ is the scaled field.

Then the width of the $1/q$ resonance can be approximated by the usual formula [1,2]

$$W_{1/q} = 4 \left(\frac{A_1}{|\Omega_0'|} \right) \Bigg|_{I=I_{1/q}} \tag{23}$$

and resonance overlap leading to global chaos can be estimated to occur [19] when the sum of the resonance island half-widths is approximately two-thirds the separation of their locations,

$$S = \tfrac{1}{2}(W_{1/q} + W_{1/q+1})/|I_{1/q} - I_{1/q+1}| \geq \tfrac{2}{3}. \tag{24}$$

Using Eqs. (22) and (23) we have determined estimates for the critical F_0 for the onset of global chaos due to resonance overlap for $\Omega/\Omega_0 < 1$ for comparison with the numerical and experimental values of Ref. [6]. For the microwave frequency, $\nu = \Omega/2\pi = 9.92$ Ghz, used in the experiments [6], the locations of classical-resonances were determined by Eq. (18), which we relate to the principle quantum numbers of the Rydberg atoms in the experiments using the Bohr-Sommerfeld quantization condition $I_{1/q} \equiv n_{1/q}$ (where $\hbar = 1$ in atomic units). The resonance island widths for $q = 1$–10 were then calculated from Eq. (23). Resonance locations and widths computed for increasing scaled microwave field n^4F are plotted as a function of initial n using dotted curves in Fig. 1. Finally, the application of the resonance overlap criterion, Eq. (24), using the "2/3 rule" predicts thresh-

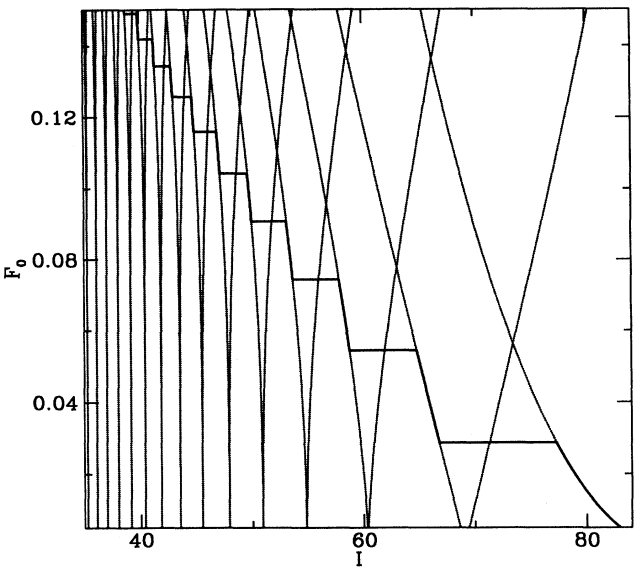

FIG. 1. The dotted lines represent the value of the action I at the top and bottom of the $1/q$ resonance (where $q = 1, \ldots 10$) for a range of scaled fields F_0. The solid line gives the threshold fields for resonance overlap as predicted by the "2/3 rule" discussed in the text.

old fields for the onset of global chaos as a function of initial action n, which are indicated by the solid curve linking the resonance zones in Fig. 1.

Below these threshold values, the perturbing field is too weak to cause overlap of the q and $q+1$ resonances, which could lead to chaotic excitation of the initial state to higher actions or quantum states and then to ionization. However, for fields above these thresholds, the overlap of adjacent resonances results in global chaos leading to ionization of the atom. A comparison of these predictions with the results of classical simulations of chaotic ionization and with experimental measurments of the threshold fields for microwave ionization shows excellent agreement in Fig. 2 with no adjustable parameters. The most notable deviations are the increased thresholds in the experiments and numerical simulations at the middle of the threshold steps associated with initial actions inside each resonance zone. However, this discrepancy is accounted for by the increased stability of the perturbed atom associated with the existence of an approximate adiabatic invariant, which is preserved by the slow turn-on of the microwave perturbation in both the experiment and simulations, as was discussed in earlier work [3].

A more serious problem indicated in Fig. 2 is that, although keeping only the A_1 contributions to the resonance widths gives good agreement for $q = 2$ and 3, the threshold fields are too large in the low-frequency limit. In fact, this approximation, which corresponds to keeping only the contributions of the permanent dipole moment in the new angle variable ϕ gives a threshold field that is a factor of 2 too big in the limit of zero frequency [20]. This discrepancy can be understood mathematically if we examine the behavior of $A_1(q)$ in the large-q limit. Using the asymptotic form of the Bessel function in $A_1(q)$ for large order and large argument,

$$J_{q-1}(3qF_0) \sim \frac{1}{\sqrt{2\pi q}} \left(\frac{3eF_0}{2}\right)^q , \tag{25}$$

we see that $A_1(q)$ converges to 0 for $F_0 < 2/3e$ as $q \to \infty$ and diverges for $F_0 > 2/3e$. So the critical field for resonance overlap can be estimated as $F_0 \approx 2/3e = 0.245$, which is nearly a factor of 2 larger than the classical scaled field threshold for static field ionization, $F_s \simeq 0.13$ [2].

The additional contributions from resonance amplitudes corresponding to other allowed index strings as well as terms arising from the perturbation of the action, Eq. (6), are necessary to *approach* the correct asymptotic limit at low scaled frequencies. For example, the amplitude given by Eq. (15) for

$$m = 2, \quad s_0 = q - 2, \quad s_{-1} = 1, \quad s_{k\neq 0,-1} = 0 \tag{26}$$

is

$$A_2^{(q)} = FV_2(I)J_{q-2}(-6qF_0)J_1\left(4J_1'(1)qF_0/(q+1)\right) . \tag{27}$$

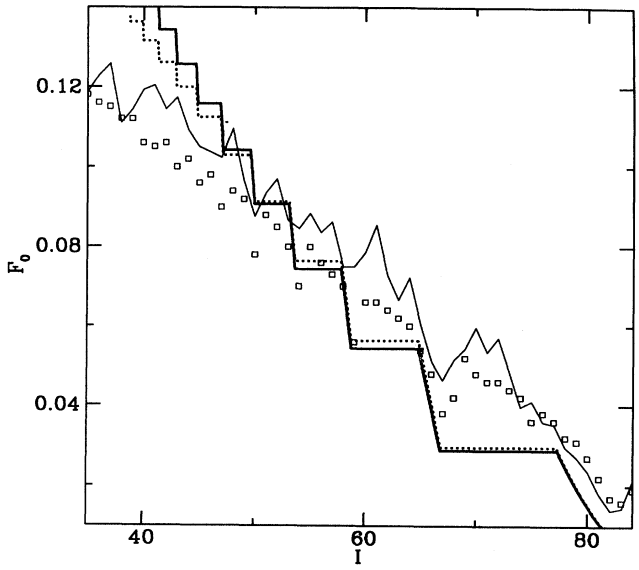

FIG. 2. Comparison of critical fields for global chaos derived from the resonance overlap criterion with experimental (thin line) [6] and numerical thresholds (points) for chaotic ionization. The solid line was obtained using only the classically computed A_1 Fourier weight, while the dashed line uses the three leading contributions to the quantum multiphoton matrix element calculated in Sec. IV in the overlap criterion. Note that the experimental thresholds are for 10% ionization and are measured only at discrete values of the scaled frequency. The experimental curve shown here is obtained by simply connecting these points. The 1D numerical simulations include time-duration, turn-on characteristics of the experiment. Readers interested in discussions on the question of dimensionality and details of this particular simulation are directed to Ref. [17] and references therein.

Using the asymptotic expansion for $J_{q-2}(-6qF_0)$, the critical field for divergent amplitudes is $F_0 \approx 1/3e = 0.123$, which is much closer to the classical value for static field ionization of 1D hydrogen atoms. Of course if we examine the asymptotic behavior of $A_3(q)$, the threshold estimate would appear to be even lower. However, the $q \to \infty$, zero frequency limit is only expected to be an asymptotic one (as in the quantum theory [21]), so extensive cancellations of the many contributing terms may be expected at any given order q.

The increasing complexity of our classical perturbation theory as the frequency decreases ultimately indicates that that our canonical transformations do not provide the most efficient or useful description of the dynamics for very low scaled frequencies. Similar conclusions were also arrived at in the work of Richards *et al.* for both quantum and classical descriptions of the very-low-frequency regime where adiabatic approximations were successfully utilized instead [22]. Consequently, the utility of our method is limited to frequencies that are not too small. In particular, we will restrict our analysis to $\Omega/\Omega_0 > 0.1$ where our converged results in Fig. 2 demonstrate that the application of the resonance overlap criterion to the subharmonic resonances for low scaled frequencies provides a good description of the classical threshold for the onset of chaotic ionization.

In Secs. III and IV we will show how an alternative method of evaluating these additional contributions to the resonance widths using the quantum mechanical multiphoton matrix elements and the Heisenberg correspondence principle can be employed to improve the very-low-frequency (large-q) estimates of the ionization thresholds. Although resonances with $\Omega/\Omega_0 = p/q$ for $p > 1$ may also be expected to reduce the ionization thresholds further, simple rules for the contributions to these terms appear to be more difficult to formulate. As these contributions are smaller than the $1/q$ resonances and our calculations keeping only the $1/q$ resonances give reasonable agreement with both the numerical simulations and the experimental data (including the low-frequency limit), we neglect them here. These additional terms are, however, considered in the recent work of both Blümel and Howard [20,23].

III. REMARKS ON THE CLASSICAL-QUANTUM CORRESPONDENCE

The Heisenberg strong correspondence principle says that the dipole transition matrix element from quantum states n to $n+m$ can be simply evaluated for large n by computing the classical Fourier component of x expressed as a function of the action-angle variables (θ, I) of the unperturbed system,

$$\frac{1}{2\pi}\int_0^{2\pi} x(\theta, I)e^{im\theta}d\theta \approx \langle n|x|n+m\rangle. \tag{28}$$

Heuristically, this powerful semiclassical relationship can be "derived" by performing a canonical transformation to appropriate action-angle variables, (I, θ), on both $x = x(\theta, I)$ and the quantum states $|n\rangle \approx e^{-in\theta}/\sqrt{2\pi}$ and $|n+m\rangle \approx e^{i(n+m)\theta}/\sqrt{2\pi}$ on the right hand side of Eq. (28). Of course quantum mechanics is not invariant under classical canonical transformations that mix the position and momentum variables. However, since the corrections involving the commutation relations of these operators are of order $\hbar$ they may be neglected in the semiclassical limit. A formal justification of the strong correspondence principle is provided in the seminal paper by Percival and Richards [11].

For single-photon transitions Eq. (28) provides a very convenient method for evaluating the quantum matrix elements for single-photon transitions between highly excited states of Rydberg atoms where the appropriate canonical transformation is to the action-angle variables of the unperturbed classical Kepler motion. For example, the dipole matrix elements, $\mu_{nn\pm m}$, for single-photon transitions between states n and $n \pm m$ are very well approximated by the classical Fourier amplitudes V_m with coefficients given by Eq. (3) [e.g., $V_1(n) \simeq -0.325n^2 \simeq \mu_{nn\pm1}$, $V_2(n) \simeq -0.11n^2 \simeq \mu_{nn\pm2}$, $V_3(n) \simeq -0.06n^2 \simeq \mu_{nn\pm3}$, ...] [7].

Remarkably, the strong correspondence principle can also be used to calculate the effective quantum matrix elements for *multiphoton* transitions between highly excited states of the one-dimensional hydrogen atom by transforming the quantum matrix elements using the new canonical variables defined by Eqs. (11). In this case we identify the quantum matrix element with the corresponding Fourier component of Eq. (13).

For example, keeping only the leading contribution to the $m = 1$ Fourier component for $I = n$,

$$A_1^{(q)}(n) = FV_1(n)J_{q-1}(3qF_0), \tag{29}$$

which gives an expression for the q-photon matrix element for quantum mechanical Rabi flopping between two states n and $n+1$ that was previously derived by Susskind and Jensen [24]. Moreover, the small argument expansion for the Bessel function reduces Eq. (29) to the multiphoton matrix element for one off-diagonal ($\Delta n = 1$) transition and $q-1$ diagonal ($\Delta n = 0$) transitions between one-dimensional hydrogen states originally derived by Bardsley and Sundaram [15]. In this latter case it is important to recognize that this quantum result only arises after the partial cancellation of individual contributions that can be many orders of magnitude larger than the final result. By contrast, the classical Fourier component, Eq. (29), delivers the correct result in a single expression. This remarkable correspondence will be explored further in the next section.

However, this term corresponds to keeping only the $k = 0$ term in the transformation to the new angle variable ϕ [Eq. (9)], which is equivalent to only transforming away the oscillations due to the permanent dipole moment $V_0 = \frac{3}{2}I^2$. The necessity of including additional terms like the $A_2^{(q)}$ term in the resonance width estimates to achieve agreement with the numerical simulations and experiment at low scaled frequencies indicates that important new, classical and quantum physics must be incorporated in the theory to describe the low-frequency,

large-q dynamics.

In particular, the additional term,

$$A_2^{(q)} = FV_2(n)J_{q-2}(-6qF_0)J_1\left(\frac{4qJ_1'(1)F_0}{q+1}\right), \quad (30)$$

corresponds to a $\Delta n = 2$ transition from n to $n+2$ involving $(q-2)$ diagonal ($\Delta n = 0$) matrix elements followed by a transition back from $n+2$ to $n+1$. In the next section we show that in the quantum theory the cancellations arising from the careful summation of a number of different terms that are orders of magnitude larger than this final term leads to a similar result for the quantum matrix element.

The reason for the classical Fourier component being orders of magnitude smaller than the individual quantum contributions is that the arguments of the Bessel functions which determine the powers of F in the matrix elements involve the derivatives of $V_k(I)$ with respect to the action $I = n$. This reduces the size of the effective q-photon matrix elements from n^{2q} to n^{q+1}. When n and q are large this reduction is enormous.

Unfortunately, a careful comparison of the quantum matrix elements with the classical Fourier coefficients shows agreement only in order of magnitude. The classical and quantum results typically differ by a numerical factor. For example, the dominant Fourier amplitudes for a three-photon transition between states with no permanent dipole moments correspond to $m = 1$, $k = 1$, $s_1 = 1$, and $k = -1$, $s_{-1} = 1$

$$A_{+1}^{(3)}(k, s_k) = FV_1J_1(-3F_0V_{-1}'/4n)J_1(3F_0V_1'/2n)\ , \quad (31)$$

and $m = -1$, $k = 1$, and $s_1 = 2$,

$$A_{-1}^{(3)}(k, s_k) = FV_{-1}J_2(-3F_0V_1'/2n)\ . \quad (32)$$

If we expand the Bessel functions in Eqs. (31) and (32) to leading order in F, we arrive at a simple expression for the multiphoton, multilevel matrix element that can be compared with the quantum results in the next section,

$$A_{+1}^{(q)} \approx 9[C_{\mathrm{Cl}}(1)F_0/2]^3/n^2 \quad (33)$$

and

$$A_{-1} \approx 9[C_{\mathrm{Cl}}(1)F_0/2]^3/n^2. \quad (34)$$

As shown later, the sum of these two contributions is exactly equal to 2/3 of the corresponding quantum mechanical three-photon matrix element given by Eq. (47).

This numerical discrepancy arises because the single canonical transformation described in Sec. II does not fully evaluate the magnitude of the resonance amplitudes. If the classical Hamiltonian, Eq. (12), is further transformed to include the perturbation of the action, Eq. (6), then additional resonance terms contribute to the resonance widths. A lengthy algebraic calculation shows that including the perturbative correction to the action in Eq. (12) to order F^3 provides the missing 1/3 contribution to the three-photon matrix element.

[Note that since the perturbation of the action does not include any additional dependence on the permanent dipole moment, V_0, only the $A_1^{(q)}$ terms, Eq. (29), corresponding to one off-diagonal $\Delta n = 1$ transition and $q-1$ diagonal $\Delta n = 0$ transition are complete.]

In general, these additional canonical transformations are very tedious. However, the Heisenberg strong correspondence principle suggests an alternative approach to evaluating the classical-resonance widths by using the quantum matrix elements to estimate the classical Fourier coefficients. After reviewing an efficient procedure for evaluating the quantum matrix elements in the next section, we will use this reverse application of the Heisenberg strong correspondence principle to improve the classical estimates for the threshold fields for low-frequency microwave ionization of highly excited hydrogen atoms in the concluding section.

IV. EFFECTIVE QUANTUM MECHANICAL MATRIX ELEMENTS

The presence of permanent dipole matrix elements, corresponding to a linear Stark effect, is peculiar to hydrogen atoms subjected to an electric field. Several studies have shown that these have to be included when computing transition rates for multiphoton processes. In the one-photon near-resonant case, inclusion of the diagonal elements does not modify the behavior within the two-level resonance or rotating-wave approximation, as the additional terms generated do not contain slowly oscillating terms. This is not, however, true in the multiphoton case where large cancellations result as a consequence of the diagonal terms.

We begin from the general perturbative expression for a resonant q-photon transition matrix element between levels labelled i and f [25]

$$M^{(q)} = 2\left(\frac{F}{2}\right)^q \sum_{l_1 l_2 \cdots l_{q-1}} \frac{\mu_{il_1}\mu_{l_1l_2}\mu_{l_2l_3}\cdots\mu_{l_{q-1}f}}{(\omega_{l_1}-\Omega)(\omega_{l_2}-2\Omega)\cdots[\omega_{l_{q-1}}-(q-1)\Omega]}, \quad (35)$$

where μ_{ij} denote dipole matrix elements between levels i and j. The prefactor 2 ensures that this general expression reduces to a simple matrix element in the single-photon limit. The peak amplitude F and frequency Ω are the external field parameters and $\omega_{l_1} = E_{l_1} - E_i$ is the energy difference between the initial level and any intermediate level l_1. For a q-photon process, the sum is over $(q-1)$ intermediate states whose energies, unlike those of the initial and final states, are not related through energy conservation. These transitions are virtual in nature as attested to by the fact that the time spent in a virtual state p, given by $\Delta t \approx (\omega_p - N\Omega)^{-1}$, is small compared with the transition time from initial to final states.

With the inclusion of permanent dipole moments, two types of transitions are possible, diagonal ones involving the same level and off-diagonal ones going across levels. In a representation involving direct products of electronic and photon states $|e;n\rangle$, where e labels the electronic state and n is the photon number, a q-photon transition from level i to f means going from $|i;q\rangle$ to $|f;0\rangle$. Taking instead the change in photon number leads to a simple way to schematize the multiphoton process. As an illustration, consider a three-photon transition in a two-level system. The level structure is as shown in Fig. 3(a), where the second label is now simply the energy denominator (defect) measured in units of the photon energy. The summation in the multiphoton matrix element (35) now corresponds to all possible paths from $|i;0\rangle$ to $|f;0\rangle$, which are shown in Fig. 3(b). The top row of diagrams may be considered as a single class, as they each involve a single off-diagonal transition from $i \to f$. The last diagram has three off-diagonal transitions and is clearly not the only one in its class. To exhaust this set one needs to go beyond the simple two-level picture, a point we shall return to later.

The procedure illustrated for the three-photon transition can easily be extended to the general q-photon case. Take the case schematized in Fig. 3(c) of this transition between levels a and b where $(q-1)$ diagonals and one off-diagonal transition are involved. Of the $(q-1)$ diagonal elements, m occur with respect to level a and the remaining $(q-m-1)$ with level b. To exhaust this class of diagrams, all possible values of m [from $0 \to (q-1)$] have to be considered. Thus, in Eq. (35), the summation over $(q-1)$ indices may be replaced by a single summation over m leading to

$$M^{(q)} = 2\left(\frac{F}{2}\right)^s \frac{1}{\Omega^{q-1}} \sum_{m=0}^{q-1} \frac{(-1)^m \mu_{aa}^m \mu_{ab} \mu_{bb}^{q-m-1}}{m!(q-m-1)\cdots[q-(q-1)]}$$
$$= \frac{2}{\Omega^{q-1}} \left(\frac{F}{2}\right)^q \frac{\mu_{ab}}{(q-1)!} \sum_{m=0}^{q-1} (-1)^m \mu_{aa}^m \mu_{bb}^{q-m-1} \frac{(q-1)!}{m!(q-m-1)!} , \tag{36}$$

where the energy differences (as seen from the three-photon case illustration) have been expressed in units of the photon energy Ω. The summation is clearly a binomial expansion leading to

$$M^{(q)} = \frac{2}{\Omega^{q-1}} \left(\frac{F}{2}\right)^q \mu_{ab} \frac{(\mu_{bb}-\mu_{aa})^{q-1}}{(q-1)!} . \tag{37}$$

Specifically for transitions between Stark states with high principal quantum number n and electric quantum number $|n-1|$ (extremal states) we use the fact that the matrix elements are well approximated by

$$\begin{aligned} \mu_{n,n} &= 3n(n-1)/2, \\ \mu_{n,n\pm1} &= -0.32(n \pm 1/2)^2, \\ \mu_{n,n\pm2} &= -0.11(n \pm 1)^2, \\ \mu_{n,n'=n\pm k} &= C_Q(k)[(n+n')/2]^2 , \end{aligned} \tag{38}$$

where the subscripts refer to initial and final states. Thus the first expression is the diagonal matrix element. Using these, a q-photon transition between neighboring extremal states (where n changes by 1) is given by

$$M_{(1)}^{(q)} = -\frac{0.32n^2}{(q-1)!} F^q \left(\frac{3n}{2\Omega}\right)^{q-1} , \tag{39}$$

while the more general transition where n changes by k leads to

$$M_{(k)}^{(q)} \approx \frac{C_Q(k)n^2}{(q-1)!} F^q \left(\frac{3nk}{2\Omega}\right)^{q-1} . \tag{40}$$

These expressions provide the first indication of the high degree of cancellation in the effective matrix element. A q-photon transition where each element is proportional to n^2 should go as n^{2q}, but what we have, as seen from our earlier classical analysis, is n^{q+1}. Once again, for large n this is a reduction of several orders of magnitude, even for modest q.

Let us now reinforce the connection between the classical Fourier weights and the quantum transition matrix elements. The matrix element (39) can be rewritten as

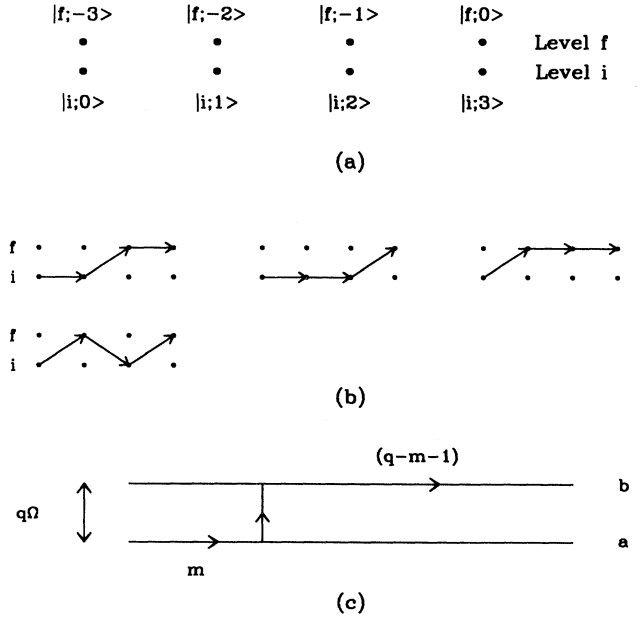

FIG. 3. (a) Level structure for a three-photon transition from levels $i \to f$ in the direct product representation. The first is the electronic state label, while the second represents the change in photon number. (b) Distinct excitation paths for three-photon transition form $i \to f$. (c) Schematic of the general q-photon matrix element with only one off-diagonal transition.

$$M_{(1)}^{(q)} = \frac{\mu_{\Delta n=1}}{(q-1)!}F^q\left(\frac{3n_0}{2\Omega}\right)^{q-1}$$
$$= C_Q(1)Fn_0^2\left(\frac{3F_0}{2\Omega_0}\right)^{q-1}\frac{1}{(q-1)!}$$
$$= C_Q(1)Fn_0^2\left[\left(\frac{3F_0q}{2}\right)^{q-1}\frac{1}{(q-1)!}\right], \qquad (41)$$

where n_0 is the initial state, the scaled variables $F_0 = Fn_0^4$, $\Omega_0 = \Omega n_0^3$, which leads to $\Omega_0 = 1/q$. Recognizing the term in square brackets as the leading term in the expansion of $J_{q-1}(3qF_0)$ establishes the correspondence with the Fourier weight A_1 computed earlier. The asymptotic behavior for large q is also recovered using Stirling's formula $(q-1)! \approx \sqrt{2\pi}q^{q-1/2}e^{-(q-1)}$ leading to

$$\lim_{q\to\infty} M_{(1)}^{(q)} = \lim_{q\to\infty}\frac{\text{const}}{\sqrt{q}}\left(\frac{3eF_0}{2}\right)^{q-1}, \qquad (42)$$

which has convergence conditions identical to those for Eq. (25).

It is clear that we have considered only a few terms of the total number of possibilities involving diagonal and off-diagonal contributions. In terms of the diagrams we have exhausted only one class, where the ones we have neglected involve fewer diagonal transitions. However, once again there are large cancellations in the effective matrix element for each class of diagrams. To verify these cancellations one must go beyond simple two-state considerations. For example, for a q-photon transition from $|i\rangle \to |f\rangle$ where we restrict n-changing to $\Delta n = \pm 1$, the conditions are

(i) Odd q: need to consider $(q-1)/2$ levels below $|i\rangle$ as well as above $|f\rangle$.

(ii) Even q: $q/2$ levels below and above $|i\rangle$ and $|f\rangle$ respectively.

This is trivially verified by considering the extreme case of q off-diagonal transitions. Relaxing the Δn restriction to include ± 2, changes these conditions to $(q-1)$ and q, respectively. General conditions can be constructed, though to do so gets increasingly more complicated.

Consistent with our earlier classical analysis, the term involving a single off-diagonal transition is the most important contribution for low-order multiphoton processes. We illustrate this by considering a three-photon transition between neighboring Stark levels where only $\Delta n = \pm 1$ transitions are considered. By our earlier arguments, we need a four-level scheme to exhibit the cancellations. We simplify the problem further by neglecting the anharmonicity in the levels and the resulting level scheme is shown in Fig. 4(a). Given the restrictions on the matrix elements, we need consider only the cases of one and three off-diagonals. The class of diagrams with one off-diagonal leads to

$$M_{(1)} = \left(\frac{F}{2}\right)^3\frac{1}{\Omega^2}\mu_{01}(3n_0)^2. \qquad (43)$$

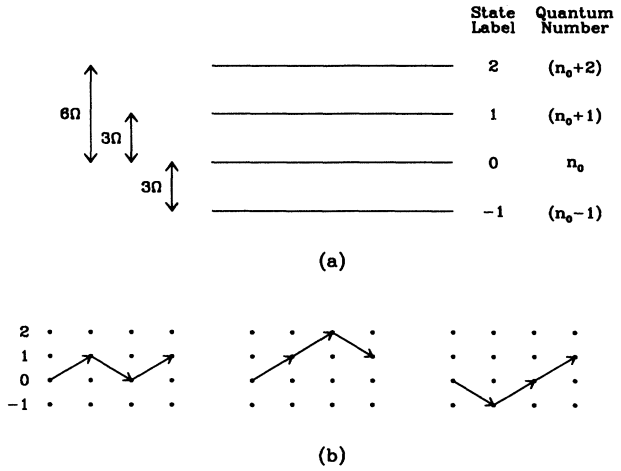

FIG. 4. (a) Four-level scheme used for calculating the three-photon contribution where all three transitions are off-diagonal. The state label that appears in the computed expressions and the corresponding quantum number are shown. Note that the state label reflects the change in quantum number, i.e., the Δn in the corresponding transition matrix element. (b) The three contributing diagrams when Δn is restricted to ± 1.

Similarly, the class with three off-diagonals shown in Fig. 4(b) leads to contributions (reading left to right)

$$2(F/2)^3\frac{1}{\Omega^2}\frac{\mu_{01}^3}{(3-1)(0-2)} = -(F/2)^3\frac{1}{\Omega^2}\frac{\mu_{01}^2\mu_{01}}{2},$$
$$2(F/2)^3\frac{1}{\Omega^2}\frac{\mu_{01}\mu_{12}^2}{(3-1)(6-2)} = (F/2)^3\frac{1}{\Omega^2}\frac{\mu_{12}^2\mu_{01}}{4},$$
$$2(F/2)^3\frac{1}{\Omega^2}\frac{\mu_{01}\mu_{0-1}^2}{(-3-1)(0-2)} = (F/2)^3\frac{1}{\Omega^2}\frac{\mu_{0-1}^2\mu_{01}}{4}. \qquad (44)$$

Summing these three competing contributions and expressing the result in a form analogous to Eq. (43), we have (to leading order)

$$M_{(3)} = -\left(\frac{F}{2}\right)^3\frac{1}{\Omega^2}\mu_{01}0.3n_0^2. \qquad (45)$$

This result is a factor of

$$M_{(3)}/M_{(1)} = 0.3/9.0 = 0.033 \qquad (46)$$

times smaller than the leading term, Eq. (43). Thus, for the three-photon case the second class of diagrams adds very little to the overall transition matrix element, which is dominated by the single off-diagonal contribution. However, as we shall illustrate later this is not the case as the order of the multiphoton process (or equivalently the order of the classical resonance) increases. We reiterate that a simple two-level scheme would account for only the first diagram in Fig. 3(b), whose contribution is nearly a factor of n_0^2 *larger* than $M_{(1)}$, giving an incorrect result.

To compare with the corresponding classical Fourier weights (31) and (32), we rewrite the sum of (44) as

$$M_{(3)} = C_Q(1)^3 \left(\frac{F}{2}\right)^3 \frac{3n^4}{\Omega^2}$$
$$= 3(q^2)[C_Q(1)F/2]^3 n^{10} = 27[C_Q(1)F_0/2]^3/n^2 , \quad (47)$$

where we have introduced scaled variables and used $\Omega_0 = 1/q = 1/3$. Recall that the classical contribution consisted of two terms that summed to a coefficient of 18, which is 2/3 of the quantum matrix element. As stated earlier, the remainder is recovered on including corrections to both action and angle variables in the classical dynamics.

A class of diagrams intermediate to the ones above involve two off-diagonals in a q-photon process. When considering transitions between neighboring levels, we have to relax the $\Delta n = \pm 1$ condition in order to get a contribution from this class. As shown in Fig. 5, once again a four-level scheme is sufficient to obtain, to leading order, the two largest contributions to a q-photon process from $0 \to 1$. By neglecting level anharmonicity, general expressions can be written down but we consider the simpler near resonant, equally spaced case when $s = r' = r = q$. The contributions from diagrams (a) and (b) are

$$M_{(a)} = 2\left(\frac{F}{2}\right)^q \frac{\mu_{02}\mu_{21}}{\Omega^{q-1}} \sum_{m_1=0}^{(q-2)} \frac{(-1)^{m_1}\mu_{00}^{m_1}}{m_1!} \sum_{m_2=0}^{(q-2-m_1)} \frac{\mu_{22}^{m_2}\mu_{11}^{m_3}}{m_3!} \frac{[2q-(m_1+m_2+2)]!}{[2q-(m_1+1)]!} ,$$

$$M_{(b)} = 2\left(\frac{F}{2}\right)^q \frac{\mu_{0-1}\mu_{-11}}{\Omega^{q-1}} \sum_{m_1=0}^{(q-2)} \frac{(-1)^{m_1}\mu_{00}^{m_1}}{m_1!} \sum_{m_2=0}^{(q-2-m_1)} \frac{(-1)^{m_2+1}\mu_{-1-1}^{m_2}\mu_{11}^{m_3}}{m_3!} \frac{(q+m_1)!}{(q+m_1+m_2+1)!} , \quad (48)$$

where $m_3 = (q - m_1 - m_2 - 2)$. Note that each contribution contains both a $\Delta n = \pm 1$ and a ± 2 term.

Evaluating these expressions for the three-photon transition considered earlier leads to

$$M_{(a)} = \left(\frac{F}{2}\right)^3 \frac{\mu_{02}\mu_{21}}{\Omega^2}\left[\frac{\mu_{11}}{5} + \frac{\mu_{22}}{20} - \frac{\mu_{00}}{4}\right] ,$$
$$M_{(b)} = \left(\frac{F}{2}\right)^3 \frac{\mu_{0-1}\mu_{-11}}{\Omega^2}\left[-\frac{\mu_{11}}{4} + \frac{\mu_{-1-1}}{20} + \frac{\mu_{00}}{5}\right] , \quad (49)$$

where the matrix elements are given in Eq. (38). Substituting and then summing these two contributions gives

$$M_{(2)} = M_{(a)} + M_{(b)} = 2\left(\frac{F}{2}\right)^3 \frac{1}{\Omega^2}\frac{27}{5} C_Q(1)C_Q(2)\, n_0^4 , \quad (50)$$

where $C_Q(k)$ are the coefficients for $\Delta n = k$ transitions and n_0 is the quantum number of the initial state. The ratio of Eqs. (50) and (43),

$$M_{(2)}/M_{(1)} = |6C_Q(2)/5| \approx 0.13 , \quad (51)$$

clearly indicates that the off-diagonal 2 term, which requires a $\Delta n = \pm 2$ matrix element, is a larger correction to $M_{(1)}$ than the $M_{(3)}$ diagrams considered earlier.

In computing these effective matrix elements we had to consider multiple excitation paths, the corresponding energy defects, and gradients in both diagonal and off-diagonal matrix elements with respect to the principal quantum number n. Despite simplifications like neglecting level anharmonicity, which allowed us to express all energy denominators as integer multiples of the photon energy, it is clear that this method for computing effective matrix elements is at best extremely tedious with increasing q. This is precisely where it is expeditious to use the strong correspondence principle.

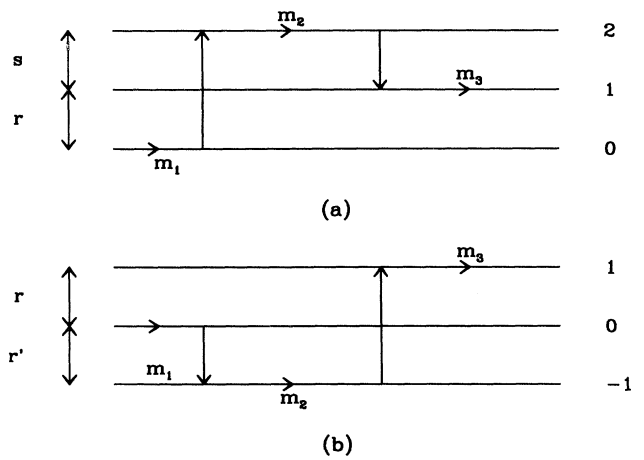

FIG. 5. Diagrams contributing to a q-photon transition between neighboring levels with two off-diagonal matrix elements. s, r, r' are the level spacings measured in units of photon energy, while m_1, m_2, and $m_3 = (q - 2 - m_1 - m_2)$ are the number of diagonal transitions at each level.

V. CONCLUSIONS

The classical Fourier coefficients provide a very useful order of magnitude estimate for the quantum matrix elements. In particular, we have shown that this remarkable classical-quantum correspondence extends to multiphoton matrix elements as well. This method for using the classical Fourier amplitudes to estimate the *multiphoton, multilevel* transition rates is not restricted to the one-dimensional hydrogen atom with its permanent dipole moments. This approach also provides a very powerful

method for estimating the multiphoton matrix elements for any quantum system where the unperturbed Hamiltonian is integrable and can be transformed to appropriate action-angle variables.

In turn, our algorithms for evaluating the quantum mechanical multiphoton matrix elements provide improved estimates of the classical Fourier amplitudes used in the resonance overlap criterion for the onset of global chaos. Table I shows the most important quantum terms for $q = 3, \ldots, 8$. For each q, every term listed has the same power of n^s and a common prefactor $(F/2)^q/\Omega^{q-1}$. The symbolic coefficient reflects the n-changing transitions involved in each contribution. For example, for $q = 3$, the most important term after the one with 2 diagonals ($T_0^2 T_1$) involves a combination of $\Delta n = 1, 2$ transitions and one diagonal ($T_0 T_1 T_2$), as shown explicitly earlier. In all the cases shown, the maximally diagonal term $T_0^{q-1} T_1$ is the largest, though for $q = 8$ both $T_0^{q-2} T_1 T_2$ and $T_0^{q-3} T_1^3$ are of comparable magnitude. In fact, $T_0^{q-3} T_1^3 > T_0^{q-1} T_1$ for $q > 10$ while $T_0^{q-2} T_1 T_2 > T_0^{q-1} T_1$ only beyond $q \approx 20$. The tabulated sizes also reflect the growth, with increasing q, of other terms involving still fewer diagonal elements. Further, the alternating sign of successive terms points to a delicate balance of competing contributions as q increases. This is consistent with the intuitive view that the approach to the static field limit of large q multiphoton processes is dominated by energy denominators.

TABLE I. Relative weights of contributions to multiphoton matrix elements of order q between neighboring states n and $n+1$. $T_{0,1,2,\ldots}$ denote transitions involving $\Delta n = 0, 1, 2, \ldots$. For example, the first symbolic coefficient represents a three-photon process involving two diagonal terms and one off-diagonal term with $\Delta n = 1$. The numerical value is the contribution from this term to the coefficient multiplying n^s. The relative size of this contribution is computed with respect to the largest term involving $(q-1)$ diagonal terms.

q	s	Symbolic coefficient	Numerical value	Relative size
3	4	$T_0^2 T_1$	-1.44	1.0
		$T_0 T_1 T_2$	0.2006	-0.139
		$T_0 T_2 T_3$	0.0021	-0.0015
		T_1^3	-0.049	0.033
		$T_1^2 T_2$	0.007	-0.0049
4	5	$T_0^3 T_1$	-1.44	1.0
		$T_0^2 T_1 T_2$	0.2897	-0.2012
		$T_0 T_1^3$	-0.1398	0.0971
		$T_0 T_1 T_2^2$	0.01079	-0.0075
		$T_1^3 T_2$	-0.00174	0.0012
		$T_1 T_2^3$	-0.00049	0.00034
5	6	$T_0^4 T_1$	-1.08	1.0
		$T_0^3 T_1 T_2$	0.281	-0.2602
		$T_0^2 T_1^3$	-0.2009	0.186
		$T_0^2 T_1 T_2^2$	-0.048077	0.0444
		$T_0 T_1^3 T_2$	0.03355	-0.031
		T_1^5	-0.0022	0.002
6	7	$T_0^5 T_1$	-0.648	1.0
		$T_0^4 T_1 T_2$	0.205509	-0.3171
		$T_0^3 T_1^3$	-0.193694	0.299
		$T_0^3 T_1 T_2^2$	-0.0461435	0.0712
		$T_0^2 T_1^3 T_2$	0.0475	-0.0733
		$T_0 T_1^5$	-0.00617	0.0095
7	8	$T_0^6 T_1$	-0.324	1.0
		$T_0^5 T_1 T_2$	0.120711	-0.3725
		$T_0^4 T_1^3$	-0.140804	0.4346
		$T_0^4 T_1 T_2^2$	-0.0334187	0.1031
		$T_0^3 T_1^3 T_2$	0.04522122	-0.1396
		$T_0^2 T_1^5$	-0.0087	0.02685
8	9	$T_0^7 T_1$	-0.1389	1.0
		$T_0^6 T_1 T_2$	0.0593	-0.427
		$T_0^5 T_1^3$	-0.0822	0.592
		$T_0^4 T_1^3 T_2$	0.0325	-0.234
		$T_0^3 T_1^5$	-0.0083	0.060

A final twist to this demonstration of classical-quantum correspondence comes from using these quantum estimates of the classical Fourier amplitudes in the resonance overlap criterion. When used to evaluate the resonance island widths used in the overlap criterion, better agreement with the numerical and experimental measurements of the ionization threshold is achieved at low scaled frequencies. This improved estimate for the onset of chaotic ionization is given by the dashed curve in Fig. 2. Extending these results to still lower scaled frequencies below $n^3\Omega = 1/8 = 0.125$ requires the further evaluation of higher-order multiphoton matrix elements. However, because of the asymptotic nature of the low-frequency limit, more and more terms must be included and the symbolic evaluation of these higher-order terms using MATHEMATICA becomes increasingly time consuming. Further, the neglect of level anharmonicity is no longer defensible. However, as noted earlier, this proliferation of terms suggests that alernative methods of describing the thresholds for destabilizing the electron at very low frequencies should be pursued instead [22].

ACKNOWLEDGMENT

This work was supported by the National Science Foundation Grant No. PHY-9214816.

APPENDIX A: RULES FOR CHOOSING THE DOMINANT CONTRIBUTIONS TO THE RESONANCE WIDTHS

For the $I^3\Omega = 1/q$ resonances, determine the strings of integers $m, k, \{s_k\}$ that satisfy the conditions

$$m + \sum_k k s_k = 1 \tag{A1}$$

and

$$1 + \sum_k s_k = q \tag{A2}$$

and evaluate the corresponding amplitudes $A_m(k, \{s_k\})$. In computing these amplitudes, $J_0(mFb_k)$ was taken to be $\approx 1 + O(F^2)$.

Example, $q = 2$*:*

m	s_0	s_1	s_{-1}	s_2	s_{-2}	$A_m(k,\{s_k\})$	
1	1	0	0	0	0	$FV_1J_1(b_0F)$	$O(F^2)$
2	0	0	1	0	0	$FV_2J_1(2b_{-1}F)$	$O(F^2)$
3	0	0	0	0	1	$FV_3J_1(3b_{-2}F)$	$O(F^2)$

(A3)

In general the leading terms in an expansion in powers of F arise from the strings with

$$\sum_k |s_k| = q - 1. \tag{A4}$$

Then for $q = 2$ the dominant terms for each m correspond to the strings $m, k = -(m-1), s_{-(m-1)} = 1$. For small F the small argument expansions of these dominant amplitudes gives

$$A_m \sim \frac{1}{m^{5/3}} \frac{m}{3(m+1)(m-1)^{11/3}} \approx \frac{1}{m^{16/3}} \text{ for large } m. \tag{A5}$$

So the $m = 1$ amplitude is the largest term for $q = 2$.

Example, $q = 3$. From Eq. (15) the leading terms of order F^3 arise from strings that satisfy Eqs. (A1) and (A2) and $\sum_k |s_k| = 2$. So either (a) one $s_k = 2$ or (b) two different $s_k = 1$ and $s'_k = 1$. In case (a) the requirement, Eq. (A1), implies that $m+2k = 1$, which is possible only for odd values of m with $k = -(m-1)/2$. In case (b) Eq. (A1) requires that $m + k + k' = 1$ or $k = -k' - (m-1)$.

m	s_0	s_1	s_{-1}	s_2	s_{-2}	$A_m(k,\{s_k\})$	
1(*a*)	2	0	0	0	0	$FV_1J_2(b_0F)$	$O(F^3)$
2(*b*)	1	0	1	0	0	$FV_2J_1(2b_0F)J_1(2b_{-1}F)$	$O(F^3)$
2(*b*)	0	1	0	0	1	$FV_2J_1(2b_1F)J_1(2b_{-2}F)$	$O(F^3)$
3(*a*)	0	0	2	0	0	$FV_3J_2(3b_{-1}F)$	$O(F^3)$

(A6)

Example, $q = 4$. From Eq. (15) the leading terms of order F^4 arise from strings that satisfy Eqs. (A1) and (A2) and $\sum_k |s_k| = 3$. So either (a) one $s_k = 3$, (b) two different $s_k = 1$ and $s'_k = 2$, or (c) three different $s_k = 1$, $s'_k = 1$, and $s''_k = 1$. In case (a) the requirement, Eq. (A1), implies that $m + 3k = 1$, which is possible for both odd and even values of m with $k = -(m-1)/3$. In case (b) Eq. (A1) requires that $m + k + 2k' = 1$. In case (c) Eq. (A1) requires that $m + k + k' + k'' = 1$.

m	s_0	s_1	s_{-1}	s_2	s_{-2}	$A_m(k,\{s_k\})$	
1(*a*)	3	0	0	0	0	$FV_1J_3(b_0F)$	$O(F^4)$
2(*b*)	2	0	1	0	0	$FV_2J_2(2b_0F)J_1(2b_{-1}F)$	$O(F^4)$
3(*b*)	1	0	2	0	0	$FV_3J_1(3b_0F)J_2(3b_{-1}F)$	$O(F^4)$

(A7)

APPENDIX B: EVALUATING MULTIPHOTON MATRIX ELEMENTS USING MATHEMATICA

Symbolic manipulation using MATHEMATICA is particularly useful both in evaluating the leading term as well as estimating the relative sizes (as shown in Table I) of contributions to the effective q-photon matrix element. We present here the schemes; the programs are available on request.

(a) Extracting the leading term for a q-photon matrix element where compact expressions are known is particularly simple. For example, consider Eq. (48), where the q-photon element involves two off-diagonal matrix elements. Given the form of the matrix elements, the summations lead to a polynomial in the principal quantum number n of the initial state. Evaluating the coefficient of the $n^{(q+1)}$ term then gives the leading behavior.

(b) This simple scheme can be modified to estimate the relative importance of contributions, involving different numbers of diagonal transitions, to the effective q-photon matrix element between neighboring levels. Consider a case where up (down) transitions with $\Delta n \leq nu$ ($nd < 0$) are included. In MATHEMATICA, the matrix elements are written as $c[\Delta n](n + \Delta n/2)^2$. The summations in the effective matrix element now result in a polynomial in coefficients $c[0], c[1], \ldots$ from which the relative weights (shown in Table I) are obtained. Note that the rules for the minimum number of levels required for exhausting classes of diagrams must be applied, i.e., if $nu = -nd = 1$, then terms involving $c[2]$ will be incorrect as we need at least $nu = 2, nd = -1$.

[1] G. M. Zaslavsky and B. V. Chirikov, Usp. Fiz. Nauk **105**, 3 (1971) [Sov. Phys. Usp. **14**, 549 (1971)].

[2] R. V. Jensen, Phys. Rev. Lett. **49**, 1365 (1982); Phys. Rev. A **30**, 386 (1984).

[3] R. V. Jensen, Phys. Scr. **35**, 668 (1987).

[4] N. B. Delone, V. P. Krainov, and D. L. Shepelyansky, Usp. Fiz. Nauk **140**, 335 (1983) [Sov. Phys. Usp. **26**, 551 (1983)].

[5] J. E. Bayfield and P. M. Koch, Phys. Rev. Lett. **33**, 258 (1974).

[6] K. A. H. van Leeuwen, G. v. Oppen, S. Renwick, J. B. Bowlin, P. M. Koch, R. V. Jensen, O. Rath, D. Richards, and J. G. Leopold, Phys. Rev. Lett. **55**, 2231 (1985); P. M. Koch, K. A. H. van Leeuwen, O. Rath, D. Richards, and R. V. Jensen, in *The Physics of Phase Space*, edited by Y. S. Kim and W. W. Zachary, Lecture Notes in

Physics 278 (Springer, New York, 1987), p. 106.
[7] J. G. Leopold and D. Richards, J. Phys. B **18**, 3369 (1985); J. Phys. B **21**, 2179 (1988).
[8] J. N. Bardsley, B. Sundaram, J. E. Bayfield, and L. A. Pinnaduage, Phys. Rev. Lett. **56**, 1007 (1986).
[9] R. Blümel and U. Smilansky, Phys. Scr. **40**, 386 (1989).
[10] G. Casati, B. V. Chirikov, I. Guarneri, and D. L. Shepelyansky, Phys. Rev. Lett. **59**, 2927 (1987).
[11] I. C. Percival and D. R. Richards, J. Phys. B **3**, 1035 (1970).
[12] R. V. Jensen, M. M. Sanders, M. Saraceno, and B. Sundaram, Phys. Rev. Lett. **63**, 2771 (1989).
[13] J. G. Leopold and D. R. Richards, J. Phys. B **27**, 2169 (1994).
[14] Bala Sundaram, Ph.D. dissertation, University of Pittsburgh, 1986.
[15] J. N. Bardsley and Bala Sundaram, Phys. Rev. A **32**, 689 (1885).
[16] S. Wolfram, *Mathematica* (Addison-Wesley, New York, 1991).
[17] R. V. Jensen, S. M. Susskind, and M. M. Sanders, Phys. Rep. **201**, 1 (1991).
[18] G. Casati, I. Guarneri, F. Izrailev, and D. L. Shepelyansky, IEEE J. Quantum. Electron. **24**, 1420 (1988).
[19] A. J. Lichtenberg and M. A. Lieberman, *Regular and Stochastic Motion* (Springer, New York, 1983), Chap. 4.
[20] R. Blümel (unpublished).
[21] See, for example, Gabriel Alvarez and Bala Sundaram, Phys. Rev. A **42**, 452 (1990), and references therein.
[22] D. R. Richards, J. Phys. B **20**, 2171 (1987); D. R. Richards *et al.*, *ibid.* **22**, 1307 (1989); P. Dando and D. R. Richards, *ibid.* **26**, 3001 (1993).
[23] J. E. Howard and M. A. Lieberman (unpublished).
[24] S. M. Susskind and R. V. Jensen, Phys. Rev. A **38**, 711 (1988).
[25] W. J. Meath and E. A. Power, J. Phys. B **17**, 763 (1984).